Crystal Structure of *Vigna radiata* Cytokinin-Specific Binding Protein in Complex with Zeatin [OA]

Oliwia Pasternak,[a] Grzegorz D. Bujacz,[a,b] Yasuyuki Fujimoto,[c] Yuichi Hashimoto,[d] Filip Jelen,[e] Jacek Otlewski,[e] Michal M. Sikorski,[a] and Mariusz Jaskolski[a,f,1]

[a] Institute of Bioorganic Chemistry, Polish Academy of Sciences, 61704 Poznan, Poland

[b] Institute of Technical Biochemistry, Technical University of Lodz, 90924 Lodz, Poland

[c] Faculty of Pharmaceutical Sciences, Teikyo University, Kanagawa 1990195, Japan

[d] Institute of Molecular and Cellular Biosciences, University of Tokyo, Tokyo 1130032, Japan

[e] Laboratory of Protein Engineering, Institute of Biochemistry and Molecular Biology, University of Wroclaw, 50137 Wroclaw, Poland

[f] Department of Crystallography, Faculty of Chemistry, A. Mickiewicz University, 60780 Poznan, Poland

The cytosolic fraction of *Vigna radiata* contains a 17-kD protein that binds plant hormones from the cytokinin group, such as zeatin. Using recombinant protein and isothermal titration calorimetry as well as fluorescence measurements coupled with ligand displacement, we have reexamined the K_d values and show them to range from $\sim 10^{-6}$ M (for 4PU30) to 10^{-4} M (for zeatin) for 1:1 stoichiometry complexes. In addition, we have crystallized this cytokinin-specific binding protein (Vr CSBP) in complex with zeatin and refined the structure to 1.2 Å resolution. Structurally, Vr CSBP is similar to plant pathogenesis-related class 10 (PR-10) proteins, despite low sequence identity (<20%). This unusual fold conservation reinforces the notion that classic PR-10 proteins have evolved to bind small-molecule ligands. The fold consists of an antiparallel β-sheet wrapped around a C-terminal α-helix, with two short α-helices closing a cavity formed within the protein core. In each of the four independent CSBP molecules, there is a zeatin ligand located deep in the cavity with conserved conformation and protein–ligand interactions. In three cases, an additional zeatin molecule is found in variable orientation but with excellent definition in electron density, which plugs the entrance to the binding pocket, sealing the inner molecule from contact with bulk solvent.

INTRODUCTION

Cytokinins are plant hormones that influence numerous physiological processes. For instance, they stimulate cell division, initiate shoot growth, and retard senescence (Mok and Mok, 1994). The naturally occurring cytokinins, with biological activities at nanomolar concentrations, are adenine analogs with different substituents at the N6 atom of the purine ring (Figure 1). In this group, the most common substituent is an isoprenoid tail, occurring for example in the first natural cytokinin to be discovered, *trans*-zeatin [N^6-(4-hydroxy-3-methyl-2-buten-1-yl)adenine] (Letham, 1963). More rarely, the adenine can be substituted with an aromatic group, as in N^6-benzyladenine. In addition to the free-base forms, cytokinins can also be present in plants as ribosides or ribotides, in which a sugar ring is attached to the N9 atom of the purine. Also, some synthetic urea derivatives show high cytokinin activity. Both purine and urea derivatives seem to bind to a common acceptor (Iwamura et al., 1980), but the structural basis of their activity has remained elusive.

The search for cytokinin receptors has led to the discovery of many cytosolic proteins capable of cytokinin binding (Romanov et al., 1990; Kobayashi et al., 2000). However, most of them bind cytokinins with low affinity. Among the potential acceptors, a 17-kD protein was detected in the soluble fraction of mung bean (*Vigna radiata*; Vr) seedlings, for which very low dissociation constants for purine- and urea-type cytokinins were initially reported (10^{-9} to 10^{-10} M) (Fujimoto et al., 1998). Those high binding affinities were determined for total protein extracts (from plant tissue or *Escherichia coli* lysate) using radioactively labeled 4PU30 [N-(2-chloro-4-pyridyl)-N'-phenylurea] and *trans*-zeatin or N^6-benzyladenine as competitors. The hydropathy profile of this cytokinin-specific binding protein (CSBP) shows that there is no signal sequence or transmembrane domain present. This supports the idea that Vr CSBP is a soluble cytosolic protein. Several other CSBPs were discovered in EST databases (one in soybean [*Glycine max*] and red kidney bean [*Phaseolus vulgaris*], two in alfalfa [*Medicago sativa*]) and in a yellow lupine (*Lupinus luteus*) cDNA library (two homologs).

Homology searches have indicated a possible classification of Vr CSBP in the structural family of pathogenesis-related class 10 (PR-10) proteins (Fujimoto et al., 1998). However, because of low amino acid sequence identity (<20%), this classification was only tentative and required experimental confirmation. PR-10 proteins are found only in plants, where they are very abundant, but their physiological function is not known. They have been

A

adenine   *trans*-zeatin   kinetin

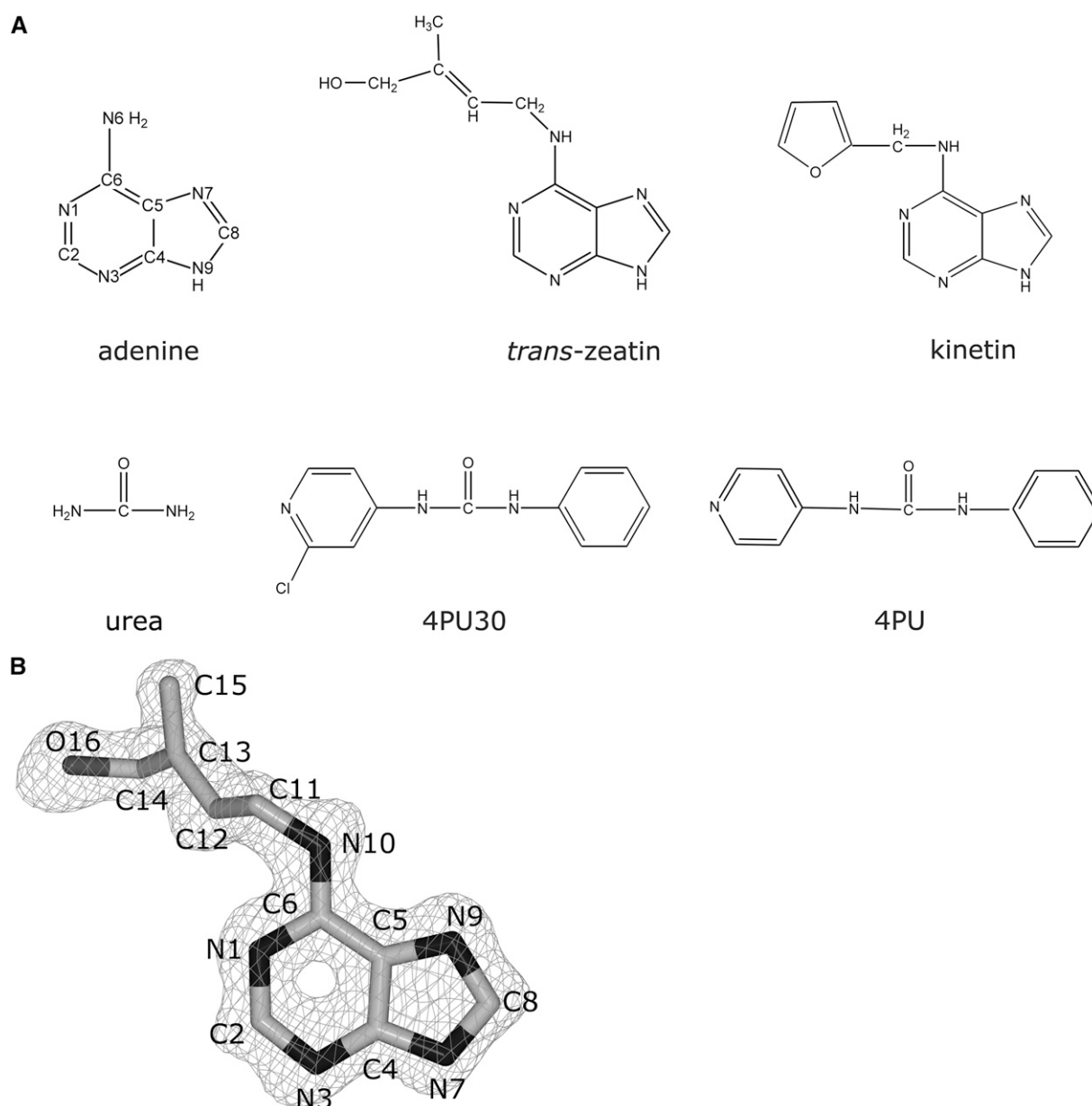urea   4PU30   4PU

B

Figure 1. Structures of Cytokinins.

(A) Selected purine- and urea-type cytokinins.
(B) A zeatin molecule (ZeaD1) as seen in the structure described here. The atom numbering, used throughout this article, is as in the Protein Data Bank entry 2FLH. The $2F_o$-F_c electron density map is contoured at the 1.2σ level.

demonstrated to play a role in plant development and during pathogen infection (van Loon and van Strien, 1999). To date, the structures of six plant PR-10 proteins have been reported (Gajhede et al., 1996; Neudecker et al., 2001; Biesiadka et al., 2002; Pasternak et al., 2005; Schirmer et al., 2005). The PR-10 fold consists of a curved β-sheet and a long C-terminal α-helix (α3), which enclose a large cavity within the protein core. An interesting feature of this fold is a Gly-rich loop (GNGGPGT), whose structural rigidity and high sequence conservation are in contrast with the high structural variability of helix α3, which is

also one of the most variable elements in amino acid sequence alignments. Recent data suggest that ligand binding may be an important part of the biological activity of PR-10 proteins. For instance, ANS (8-anilino-1-naphthalenesulfonic acid) displacement assays revealed that a birch (*Betula verrucosa*) pollen PR-10 protein (Betv1) may bind many physiologically relevant ligands (Mogensen et al., 2002). It has been suggested that the ligand binding function of PR-10 proteins might be controlled by the sequence and conformation of helix α3 (Pasternak et al., 2005). In agreement with these speculations is the observation

by Markovic-Housley et al. (2003) that the Y-shaped cavity of Betv1 can be occupied by two deoxycholate molecules. The structural similarity of deoxycholate and brassinosteroids, which are ubiquitous plant steroid hormones, may indicate a phytosteroid hormone carrier function.

Here, we present the atomic resolution structure of the Vr CSBP, establishing the folding class of cytokinin-specific binding proteins. The structure confirms that CSBPs are indeed members of one structural group with PR-10 proteins and, in this way, indirectly reinforces the notion that plant PR-10 proteins have evolved to bind small-molecule ligands. The structure has been determined in complex with zeatin. It reveals conserved binding of the zeatin ligand at the bottom of the binding cavity. The binding pocket can accept another copy of the hormone molecule to plug the entrance to the cavity and seal the conserved binding site from contact with solvent. In addition, we have re-examined the binding constants of Vr CSBP with various cytokinins, showing them to be significantly lower than originally reported. The K_d values determined by isothermal titration calorimetry (ITC) and ANS displacement range from 10^{-6} M for 4PU30 to 10^{-4} M for zeatin.

RESULTS AND DISCUSSION

Cytokinin Binding Assays

Vr CSBP binding of zeatin, 4PU30, kinetin (N^6-furfuryladenine), and 2iP [6-(γ,γ-dimethylallyl-amino)purine] was studied using an ANS displacement assay as described for Betv1 (Mogensen et al., 2002). Free ANS is a very weak fluorophore that upon CSBP binding displays a massive increase in fluorescence intensity, with a change of emission maximum from 520 to 480 nm. Titration of ANS in 10 mM MOPS, pH 7.0, with increasing concentration of CSBP provided a K_d value of 32.5 $\pm$ 1.4 μM (Figure 2, Table 1). A similar value of 18.5 $\pm$ 5 μM was obtained for the Betv1/ANS complex (Mogensen et al., 2002). As expected, titration of the preformed CSBP/ANS complexes with selected

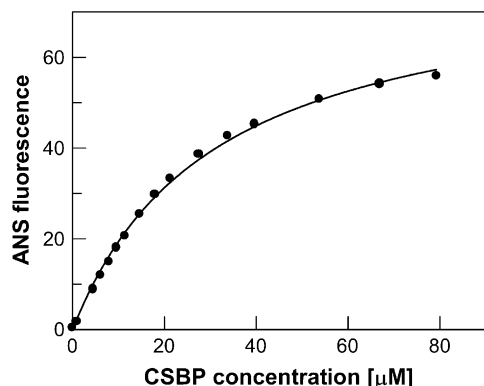**Figure 2.** ANS Binding to CSBP.

Titration of 5 μM ANS in 10 mM MOPS buffer, pH 7.0, with Vr CSBP at 20°C. The line represents the best fit to Equation 1. The calculated K_d value is 32.5 $\pm$ 1.4 μM. ANS was excited at 360 nm, and emission at 480 nm was measured.

Table 1. Binding Affinity of Vr CSBP and the Studied Ligands

Ligand	Assay	K_d (μM)	n
ANS	Direct	32.5 $\pm$ 1.4	1.24
	ADA	161 $\pm$ 18	0.97
Zeatin	ITC	106 $\pm$ 12	1.09
	ADA	148 $\pm$ 14	1.15
Zeatin H$^+$	ITC	56 $\pm$ 7	0.92
4PU30	ADA	1.3 $\pm$ 0.1	1.05
2iP	ADA	11.5 $\pm$ 1.3	0.96
Kinetin	ADA	64.1 $\pm$ 4.7	0.98

Direct indicates direct measurement of ANS fluorescence. ADA, ANS displacement assay; n, stoichiometry (ITC experiments) or Hill slope (fluorimetric titrations).

ligands caused a decrease of the fluorescence signal (Figure 3A). The raw data were analyzed as described in Methods to yield the K_d values shown (Figure 3, Table 1). The binding affinities for the selected ligands cover the micromolar range and are lower for zeatin and kinetin, moderate for 2iP, and high for 4PU30. The calculated Hill slopes of 0.97, 0.98, 0.96, and 1.05, respectively, indicated 1:1 stoichiometry.

As Trp and ANS are a suitable pair for fluorescence resonance energy transfer, parallel to the excitation of the ANS molecule at 360 nm, the unique Trp-19 of Vr CSBP was excited and the emission of ANS fluorescence at 480 nm was recorded. Fitting the fluorescence resonance energy transfer data to Equation 2 and then Equation 3 (see Methods) yielded K_d values very similar to those obtained from direct ANS fluorescence measurements.

To verify the fluorescence-derived data, we used direct measurement of all of the thermodynamic parameters of CSBP–ligand interactions. Because of very low solubility of the remaining ligands, only zeatin binding was characterized by ITC. CSBP–zeatin binding is exothermic with 1:1 stoichiometry ($n = 1.09$), K_d of 106.8 μM, ΔH of -13.7 kJ·mol^{-1}, and ΔS of 29.1 J·mol^{-1}·K^{-1} (Table 1, Figure 4). Titration of CSBP with protonated zeatin gave only a slightly lower K_d of 56.2 μM but with markedly different ΔH and ΔS contributions (-5.7 kJ·mol^{-1} and 61.9 J·mol^{-1}·K^{-1}, respectively), suggesting a clear example of enthalpy/entropy compensation. We have analyzed the calorimetric experiments by fitting the raw data to independent- and multiple-sites models as well as to a cooperativity model. Only the independent-sites model provided meaningful results with 1:1 stoichiometry, whereas the multiple-sites and cooperativity models, despite the higher number of variables, produced very poor statistics.

The discrepancy between these K_d values and those reported previously (Fujimoto et al., 1998) can be attributed to such aspects of the earlier experiments as the use of total protein extracts (instead of purified CSBP) and the application of radioactively labeled ligand molecules, both of which (especially in combination) can introduce large errors into the estimated dissociation constants.

Overall Structure of Vr CSBP

The Vr CSBP has a fold typical of the PR-10 protein family. It consists of a seven-stranded antiparallel β-sheet that forms a
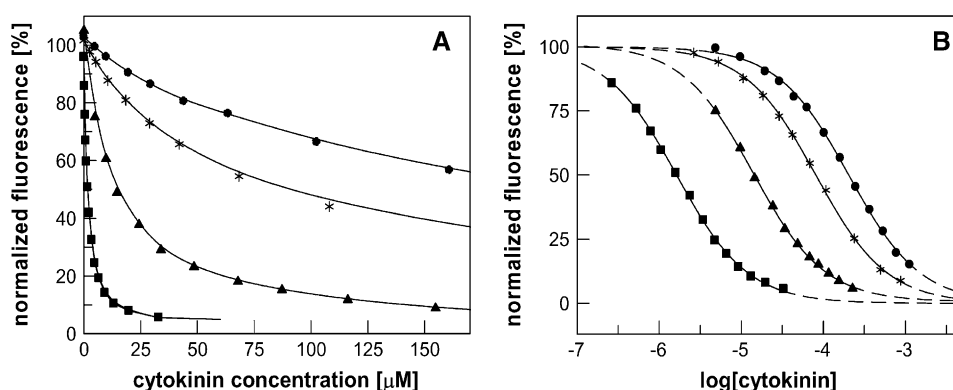
Figure 3. Binding of Zeatin, 4PU30, 2iP, and Kinetin to Vr CSBP.

Titration of 8.5 μM ANS complexed with 5.84 μM Vr CSBP in 50 mM Tris, pH 7.0, at 20°C, with zeatin (closed circles), 4PU30 (closed squares), 2iP (closed triangles), and kinetin (stars).

(A) Experimental raw data. Lines are drawn to guide the eye.

(B) Fitting of the experimental data to Equation 2. The K_d values were calculated using Equation 3 and are given in Table 1. ANS was excited at 360 nm, and emission at 480 nm was measured. The fluorescence signal was normalized to reflect 0 to 100% of ligand binding.

grip around a long C-terminal helix, α3. Between these two main structural elements, an internal cavity is present, closed at one end by two short helices, α1 and α2, which join the β1 and β2 strands, forming the opposite edges of the β-sheet (Figure 5). The other end of the channel is closed by loop L9, which connects the β-sheet with the C-terminal helix. The asymmetric unit contains four protein molecules, designated A, B, C, and D. They segregate into pairs with pseudo-twofold symmetry (AB and CD), within which the monomers form similar interactions through their α1/α2 regions. Those dimers interact further using their L5/L7/L9 loops, creating in effect a layer of roughly coplanar molecules. These interactions are most likely a crystallographic artifact, because Vr CSBP is monomeric in solution, as confirmed by size-exclusion chromatography (data not shown).

The recombinant protein consists of 155 amino acids, but a few residues are missing from the C terminus of the model (A, four; B, two; C, three; D, one). Also, part of loop L9 is not visible in molecule A. Of the 620 amino acid residues in the asymmetric unit, 34 have their side chains modeled in two conformations.

Apart from the 4 protein monomers, the asymmetric unit contains 9 zeatin molecules, 2 metal cations, and 676 modeled water molecules. Generally, the zeatin binding sites are formed inside the cavity within the protein core. Four zeatin ligands are found in conserved orientation in the A, B, C, and D protein molecules. In molecules A, B, and D, there is a second ligand in the cavity, found in variable orientation. The remaining two zeatin molecules are located outside of the binding pockets, between protein chains. Within loop L9 of molecules B and C, a metal cation is found. The coordination spheres have octahedral geometry (in molecule C, one water ligand is missing), and both include the Ile-126 carbonyl O atom. The cations have been interpreted as Na$^+$ based on satisfactory refinement of their B-factors ($\sim$29 Å^2), which are comparable with those of the coordinating O atoms (27 Å^2), and on the Na$^+$. . .O distances (2.4 to 2.9 Å). Final confirmation of the identity of the metal was provided by bond valence tests (Brese and O'Keeffe, 1991; Nayal and Di Cera, 1996) for the cation with the complete coordination sphere. The

presence of Na$^+$ cations is a crystallographic artifact attributed to the composition of the purification and crystallization buffers (elution with NaCl and precipitation with 1.2 M Na-citrate).

Zeatin Binding

The zeatin binding sites are formed within the large cavity inside the protein molecule, between the β-sheet and the C-terminal helix α3. In each protein molecule, one zeatin ligand, referred to as the inner ligand, is bound in identical orientation deep in the binding cavity. In three protein molecules (A, B, and D), an additional zeatin ligand (referred to as the outer ligand) is found at the entrance to the binding cavity, with partial exposure to solvent (Figure 6). The labels used for the ligand molecules consist of a protein chain label followed by the number 1 or 2 for the inner or outer zeatin, respectively (e.g., in protein molecule A, there are two zeatin molecules, ZeaA1 and ZeaA2). The crystallographic zeatin molecules found between the protein chains are labeled using the chain names (e.g., ZeaCC for the ligand bound between two crystallographic copies of chain C).

The inner zeatin molecules in CSBP copies A, B, and D are completely inaccessible to bulk solvent (Figures 6E and 6F) but are sealed off in their cavities with two occluded water molecules (Figure 6C). ZeaC1, in the binding site with single occupation, has direct contact with bulk water (Figure 6G) with a solvent-accessible area of 31.3 Å^2 (calculated in AREAIMOL [Lee and Richards, 1971]), as the entrance to the cavity is not sealed with a second ligand molecule. The four inner zeatin molecules have the same conformation and hydrogen bonding (Figure 7, Table 2). The nitrogen atom N3 interacts with the Thr-139 Oγ1, whereas the nitrogen atoms N10 and N9 form hydrogen bonds with Glu-69 (ZeaN10. . .Oε1Glu69 and ZeaN9. . .Oε2Glu69). Interestingly, although Glu-69 has a double conformation in chain B, this pattern of interactions with ZeaB1 is retained. The nitrogen atoms N1 and N7 interact with occluded water molecules. The exception is N1 from ZeaB1, which does not have a hydrogen bonding partner. This is a consequence of the different orientation of the
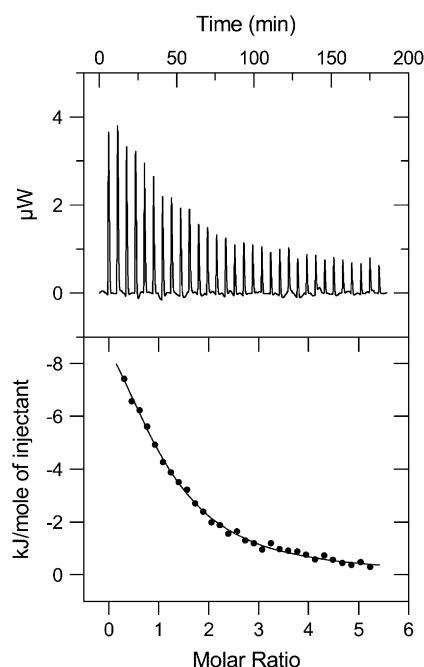
Figure 4. Calorimetric Titration of Vr CSBP with Zeatin.

The top panel shows raw heat data corrected for baseline drift obtained from 31 consecutive injections of 2.93 mM zeatin into the sample cell (1.05 mL) containing 0.148 mM Vr CSBP in 20 mM phosphate buffer, pH 6.5, at 20°C. The bottom panel shows the binding isotherm created by plotting the heat peak areas against the molar ratio of zeatin added to Vr CSBP present in the cell. The heats of mixing (dilution) were subtracted. The line represents the best fit to the model of n independent sites. The CSBP–zeatin binding is exothermic with 1:1 stoichiometry ($n = 1.09$), K_d of 106.8 μM, ΔH of -13.7 kJ$\cdot$mol^{-1}, and ΔS of 29.1 J$\cdot$mol$^{-1}\cdot$K^{-1}.

second zeatin molecule, which positions its hydrophobic tail in place of the N7 group, thus repelling water molecules from its neighborhood. Generally, the hydroxyl group at the tip of the aliphatic tail of the inner ligand forms two hydrogen bonds, with Tyr-142 Oη and Leu-22 O. However, in molecule C, an additional water molecule is incorporated, forming a hydrogen bond with Tyr-142 Oη. Moreover, both Tyr-142 and the extra water molecule are modeled in two alternative conformations. Thus, the O16 atom of ZeaC1 does not interact with Tyr-142 Oη but with the water molecule at position A, whereas the hydrogen bonding interaction to Leu-22 O is retained. Additionally, the inner zeatin molecules are stabilized by extensive van der Waals contacts with aromatic side chains (Figure 7) lining the bottom of the binding cavity (Phe-26, Phe-56, Phe-102, Tyr-98, and Tyr-142).

The outer binding site appears to have low affinity for the zeatin molecule, as it is left unoccupied in molecule C, and is nonspecific in the sense that it allows the ligand to assume different orientations. In molecules A and D, the two ligand molecules in each cavity are oriented toward each other with their purine rings (Figures 6A and 6E), whereas in molecule B, the zeatin molecule ZeaB2 is rotated, with its tail pointing toward the purine ring of the inner molecule (Figures 6B and 6F). It is likely that the outer zeatin ligands are a crystallographic artifact, but it is interesting that

they were incorporated in the binding cavity at very low (threefold) molar excess of zeatin over CSBP. We note that the outer ligand plugs the entrance to the cavity, shielding the invariable hormone molecule from contact with bulk solvent.

Surprisingly, none of the ligand molecules interacts with the Gly-rich loop L4, contrary to earlier speculations about its role in ligand binding (Biesiadka et al., 2002). Also, the loop does not seem to be a possible route by which the ligand could enter the cavity, as this entrance is blocked by the two short helices α1 and α2 (Figure 5). The most likely path for zeatin entry is through a cleft formed by the C-terminal helix α3 and loops L3, L5, and L7, assuming that the inner ligand enters first and the outer one plugs the cavity afterward. In a sense, therefore, the location of two ligands in the binding pocket can map the path of the inner ligand from the point of entry to its final destination.

Conformation of the Ligands

All zeatin molecules for which the position of the O16 atom could be modeled have evident *trans* configuration (Figures 1 and 8). The rotation of the exoamino N10 substituent is similar, with the isoprenoid tail distal to the imidazole ring, but a degree of conformational freedom is visible. Two types of zeatin conformation can be identified. The dominating conformation, characterized by the torsion angles C6-N10-C11-C12 and N10-C11-C12-C13 of approximately -70 and $-150°$, respectively, is observed for all inner zeatin molecules as well as for the outer ZeaA2 and ZeaD2 molecules, bound in the head-to-head orientation. The third outer zeatin (ZeaB2), bound in a head-to-tail manner, has a different conformation, with the torsion angle N10-C11-C12-C13 of approximately $-75°$. This rotation around the C11-C12 bond is accompanied by a change of the orientation of the hydroxyl group. These conformational changes allow the ZeaB2 (and ZeaAB) molecules to avoid steric clashes that would be inevitable in the other form.
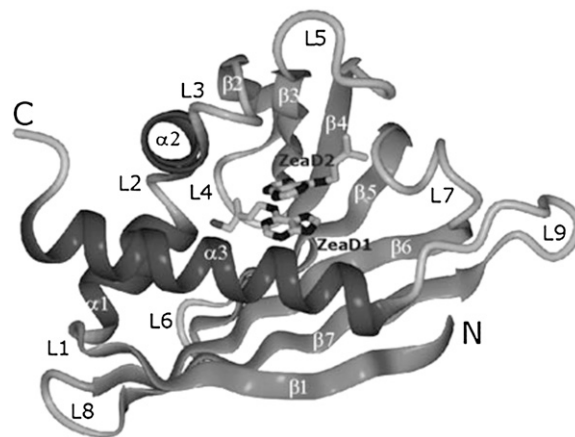

Figure 5. Overall Fold of the Vr CSBP with Annotation of Secondary Structure Elements.

The molecule (D) is shown with its two zeatin ligands (ZeaD1, inner; ZeaD2, outer) in the binding pocket.
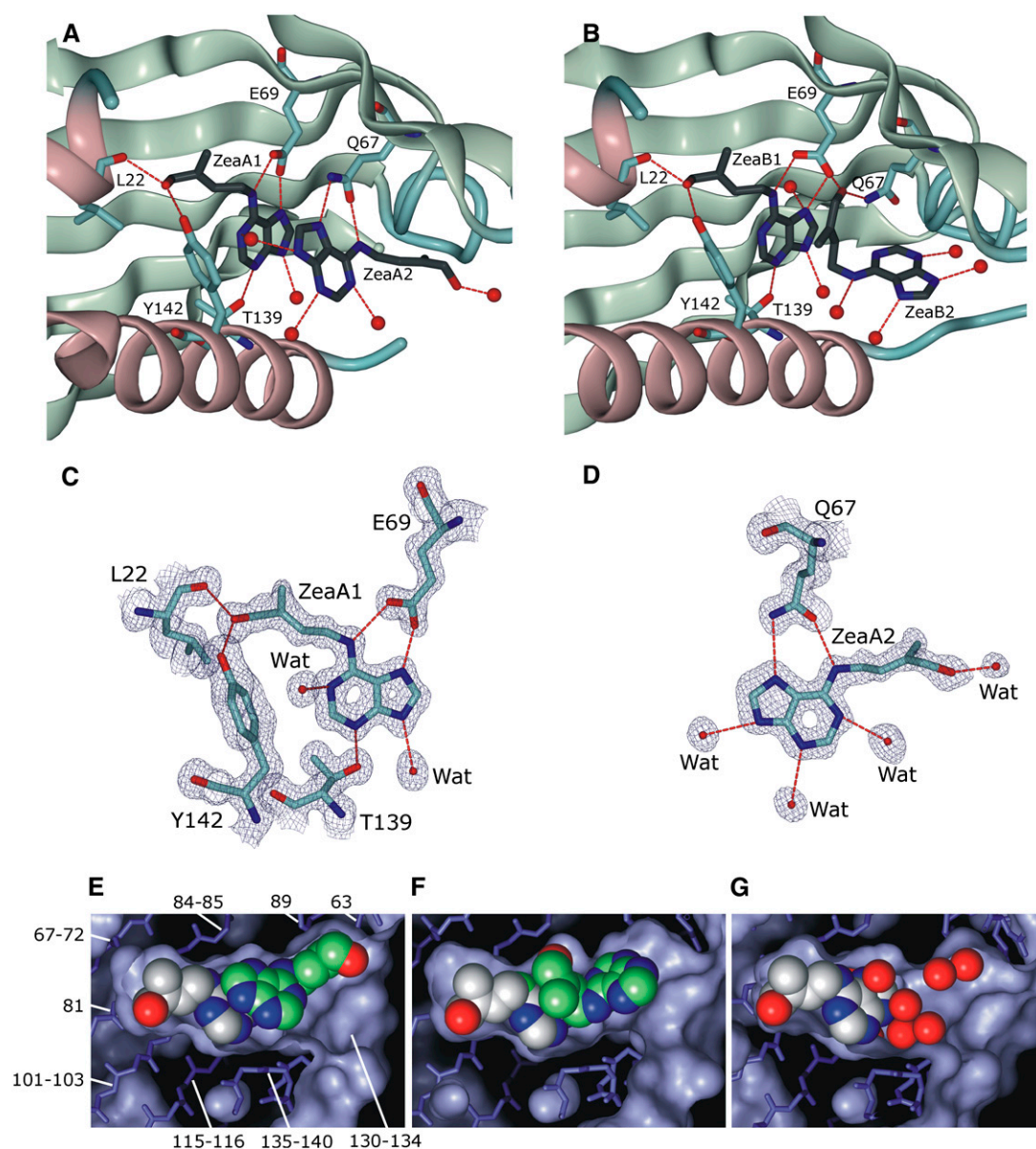
Figure 6. Zeatin Ligands in the Binding Sites.

(A) The ligand binding cavity in molecule A. This pattern is also seen in molecule D, with minor differences. Note the head-to-head (purine-to-purine) orientation of the zeatin ligands.

(B) The same view for molecule B. Here, the outer zeatin molecule (ZeaB2) is rotated, with its isoprenoid tail pointing toward the purine ring (head-to-tail) of the inner ligand (ZeaB1).

In **(A)** and **(B)**, part of the protein (Phe-26 to Thr-52) has been omitted for clarity. For viewing into the binding pocket, the molecule in Figure 5 has been rotated $-90°$ around the horizontal axis and then $-45°$ around the vertical axis.

(C) and **(D)** The inner (ZeaA1 **[C]**) and outer (ZeaA2 **[D]**) zeatin ligands of molecule A are shown in a $2F_o$-F_c electron density map contoured at the 1.2σ level. Only one alternative is shown for residues modeled in dual conformation.

(E) to **(G)** The close fit of the zeatin molecules in the internal cavities of molecules A, B, and C. The protein is shown in a cutaway surface representation with the main chain in a stick model. The ligands are represented by space-filling models with N atoms colored blue, O atoms colored red, and C atoms colored white or green for the inner or outer binding site, respectively. The cavity is filled by head-to-head–oriented ligands in molecule A **(E)**, by head-to-tail–oriented ligands in molecule B **(F)**, and by a single (inner) ligand in molecule C **(G)**. The entrance to the cavity in molecule C is filled with ordered water molecules (red spheres).
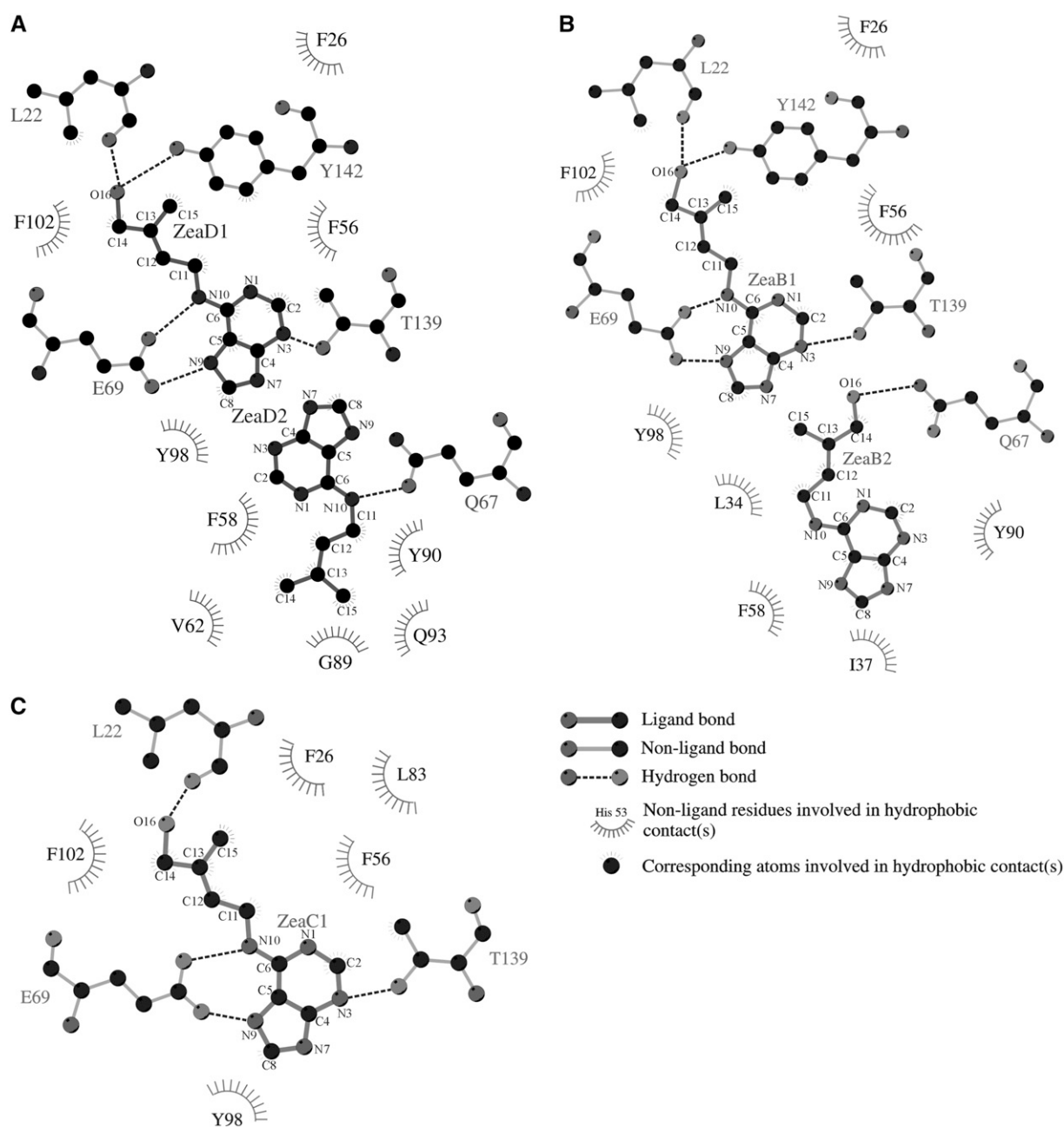
Figure 7. LIGPLOT (Wallace et al., 1995) Representations of the Interactions of the Zeatin Ligands in the Binding Pocket of the CSBP Molecules.

(A) Molecule D with two zeatin ligands bound head-to-head (a nearly identical diagram for molecule A is not shown).
(B) Molecule B with two zeatin ligands bound head-to-tail.
(C) Molecule C with only one (inner) zeatin ligand in the binding pocket.
Only interactions with protein atoms are shown. Water molecules forming additional hydrogen bonds with the zeatin molecules have been omitted for clarity.

CSBP and the PR-10 Protein Family

PR-10 proteins are abundant in plants but have no sequence homologs in other organisms. They have been implicated in plant defense and development programs, but their precise function is not known despite the accumulating structural data (Gajhede et al., 1996; Neudecker et al., 2001; Biesiadka et al., 2002;

Pasternak et al., 2005; Schirmer et al., 2005). Based on very low sequence identity (<20%) with classic PR-10 proteins, it has been hypothesized that proteins belonging to the CSBP family might also fall into the PR-10 structural class. The structure described here confirms those tentative assumptions. CSBP has all of the structural elements defining the PR-10 class, including

Table 2. H Bonding Interactions of Inner Zeatin Molecules Located in the Binding Cavity, with Corresponding Donor...Acceptor Distances in Parentheses (Å)

Atom	ZeaA1	ZeaB1	ZeaC1	ZeaD1
N1	Wat-83O (3.0)	–	Wat-358O (3.2)	Wat-132O (3.0)
N3	Thr-139Oγ1 (2.8)	Thr-139Oγ1 (2.7)	Thr-139Oγ1 (2.7)	Thr-139Oγ1 (2.8)
N7	Wat-49O (2.8)	Wat-39O (2.7)	Wat-105O (2.8)	Wat-59O (2.8)
		Glu-69Oε2_A (2.6)		
N9	Glu-69Oε2 (2.5)	Glu-69Oε2_B (2.7)	Glu-69Oε2 (2.8)	Glu-69Oε2 (2.6)
		Wat-74O (3.1)		
N10	Glu-69Oε1 (2.8)	Glu-69Oε1_A (2.8)	Glu-69Oε1 (2.8)	Glu-69Oε1 (2.8)
		Glu-69Oε1_B (3.0)		
O16	Leu-22O (2.7)	Leu-22O (2.7)	Leu-22O (2.6)	Leu-22O (2.6)
	Tyr-142Oη (2.8)	Tyr-142Oη (2.6)	Wat-125O_A (2.9)	Tyr-142Oη (2.7)

_A and _B denote residues with dual conformation.

the seven-stranded β-sheet, the C-terminal α-helix, the loop system with the Gly-rich loop, and the internal cavity (Figure 9).

In Table 3, the root-mean-square (rms) deviation values for the superpositions of the Cα atoms of Vr CSBP and PR-10 proteins are listed. Although all of the monomers of Vr CSBP present in the asymmetric unit have the same general fold, the rms deviations calculated for the corresponding Cα pairs are ~0.5 Å, with a maximum Cα-Cα distance of ~2 Å. For a crystal structure determined at 1.2 Å, these deviations should be treated as indicating some small but significant differences. More specifically, the highest discrepancies (>0.6 Å) are observed between the protein molecules harboring two ligands in head-to-head orientation (A and D) and molecule C with only one zeatin ligand (Table 3). The discrepancy is smaller (~0.4 Å) for molecules C and B. The CSBP molecules A and D, with identical zeatin binding (head-to-head), show the smallest rms deviation (0.3 Å).

Superposition of Vr CSBP on the known PR-10 structures deposited in the Protein Data Bank shows conservation of the canonical PR-10 fold but also reveals significant structural differences. A detailed analysis shows that the β-sheet, although highly curved, is very conserved and rigid. The differences are concentrated within helix α3 and in the loop regions. Helix α3 is generally the most diverse fragment also among classic PR-10 proteins (Biesiadka et al., 2002). The helices differ not only in conformation, with the most drastic example furnished by *Lupinus luteus* (Ll) PR-10.2A, in which the helix is kinked by 60° (Pasternak et al., 2005), but also in position, as in Betv1, in which the entire helix is shifted about one coil along its axis. It has been postulated that the variability of helix α3 has evolved as a way of regulating the specificity of the numerous PR-10 proteins toward their ligands through changes in the volume and shape of the binding cavity. Furthermore, the loops L3, L5, and L7 located at the entrance to the cavity show high structural divergence as well and could be additional elements of specificity control.

Although the structural variability among classic PR-10 proteins is quite high (average rms deviation of 1.4 Å), the difference between Vr CSBP and the PR-10 group (Table 3) is even higher (average of 1.6 Å for fewer Cα matches). This finding indicates that some significant structural differences are characteristic only for the CSBP. The regions that are not conserved between

CSBP and classic PR-10 proteins include the C terminus and loop L8. However, the most prominent deviation, amounting to 12 Å, is found at loop L9, which is the hinge connecting helix α3 with the rest of the structure (Figure 9A). Within classic PR-10 proteins, differences in this region do not exceed 3 Å. Moreover, in Vr CSBP, the L9 loop is longer because one N-terminal coil of helix α3 became unwound.

The structural changes of loop L9 are correlated with the atomic interactions at the N terminus. Classic PR-10 proteins have a conserved N-terminal Gly-1 residue (Figure 9C) whose
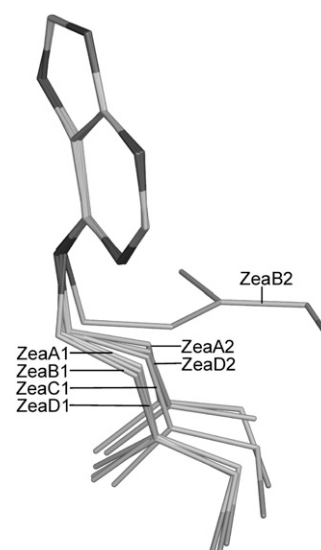
Figure 8. Conformations of the Zeatin Molecules.

Two distinct conformations of the ligand molecules bound in the binding pocket can be distinguished. All of the inner zeatin molecules as well as the outer ones with head-to-head orientation populate the most abundant conformation. The outer ZeaB2 molecule (bound in head-to-tail mode) has a different value of the N10-C11-C12-C13 torsion angle. The purine rings of the zeatin molecules were superimposed in LSQKAB (Kabsch, 1976).
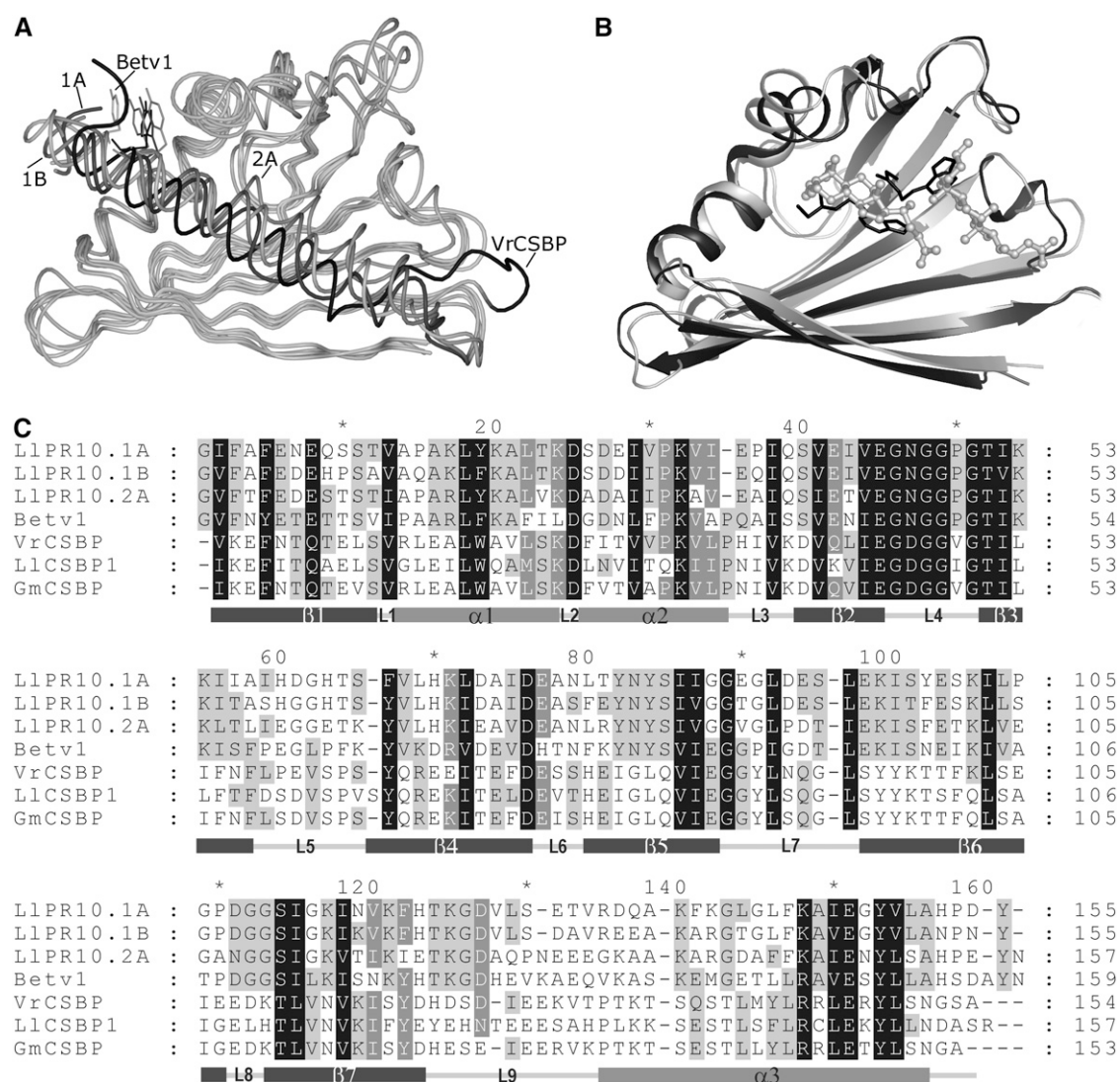
Figure 9. Comparison of Vr CSBP with PR-10 Proteins.

(A) Superposition of the Cα atoms of Vr CSBP (molecule A), Ll PR-10.1A (1A), Ll PR-10.1B (1B), Ll PR-10.2A (2A), and Betv1. The position of Tyr-149 (Tyr-148 in Ll PR-10.1 and Tyr-150 in Betv1) is indicated (stick model) to show the axial shift of helix α3 in Betv1. Calculations were made in ALIGN (Cohen, 1997).

(B) Superposition of Vr CSBP molecule B (dark gray) with two zeatin molecules bound head-to-tail (black line) on Betv1 (light gray) in complex with two deoxycholate molecules (ball-and-stick model) (Markovic-Housley et al., 2003). Helix α3, covering the binding pocket in this view, has been removed for clarity.

(C) Amino acid sequence alignment of selected CSBP and PR-10 proteins. Secondary structure elements are indicated as present in Vr CSBP. The level of conservation is expressed by the darkness of the lettering background. Note the conservation of the amino acid sequence in the Gly-rich loop L4 and the highly divergent sequence patterns at the end of loop L9 and at the N terminus of helix α3. Calculations were made in ClustalW (Thompson et al., 1994). Betv, *Betula verrucosa*; Gm, *Glycine max*; Ll, *Lupinus luteus*; Vr, *Vigna radiata*.

free −NH$_3^+$ group is involved in H bonding interactions stabilizing the L9 loop (Biesiadka et al., 2002). The Vr CSBP sequence lacks this Gly residue and starts with a Val corresponding to Val/Ile-2 of the PR-10 proteins (Figure 9C). In three copies of the Vr CSBP molecule (A, B, and C), extra electron density was found at the N terminus, indicating that a Met residue introduced by the bacterial expression system has not been fully excised by the bacterial methionyl aminopeptidase. In the structure described

here, the Met residue (probably present with partial occupancy) shows a degree of disorder and its side chain could not be properly modeled beyond Cβ. It is obvious, however, that the visible main chain of this residue is not involved in any interactions with loop L9 in its CSBP-specific conformation (Figure 9A). Incomplete removal of the initiator Met residue, therefore, is not expected to influence the overall structure stability or ligand binding.

Table 3. Superpositions of Crystallographic Models of CSBP and PR-10 Proteins, Characterized by rms Deviation (Å)/Number of Cα Pairs

Protein	Vr CSBP (B)	Vr CSBP (C)	Vr CSBP (D)	Ll PR-10.1A	Ll PR-10.1B (A)	Ll PR-10.2A (A)	Betv1
Vr CSBP (A)	0.53/141	0.63/137	0.31/137	1.66/131 (19%)	1.40/131 (21%)	1.40/118 (19%)	1.46/126 (23%)
Vr CSBP (B)	–	0.43/145	0.42/141	1.67/138	1.39/138	1.46/126	1.41/134
Vr CSBP (C)	–	–	0.54/144	1.76/134	1.53/133	1.59/124	1.72/134
Vr CSBP (D)	–	–	–	1.73/137	1.53/135	1.62/126	1.66/133
Ll PR-10.1A	–	–	–	–	1.18/147 (76%)	1.42/145 (58%)	1.40/135 (43%)
Ll PR-10.1B (A)	–	–	–	–	–	1.28/149 (59%)	1.55/143 (42%)
Ll PR-10.2A (A)	–	–	–	–	–	–	1.39/133 (44%)

Amino acid sequence identities are shown (in parentheses) for the compared proteins. The results are shown for the four copies of Vr CSBP (this work), for three yellow lupine PR-10 proteins (Ll PR-10.1A, molecule A of Ll PR-10.1B [Biesiadka et al., 2002], and molecule A of Ll PR-10.2A [Pasternak et al., 2005]), and for birch pollen allergen, Betv1 (Gajhede et al., 1996). Calculations were made in ALIGN (Cohen, 1997) using all Cα atoms (auto mode).

Ligand Binding in Vr CSBP and Betv1

To date, the only described crystal structure of a PR-10 protein with bound ligand is that of Betv1 in complex with deoxycholate (Markovic-Housley et al., 2003). Although deoxycholate is an artificial ligand for a plant protein, some similarities can be noticed in the binding modes of CSBP and Betv1. In both cases, the binding occurs in the cavity and there are two ligand molecules bound in tandem (Figure 9B). However, the deoxycholate molecules could not be modeled in the cavity of Vr CSBP after superposition on the Betv1 complex structure because of steric clashes and incompatible amino acid properties. The steric hindrance results from the presence of several aromatic residues in Vr CSBP (Phe-56, Tyr-90, Tyr-98, and Tyr-142) directed toward the two binding sites and from the position of loop L9. These changes decrease the volume of the cavity, thus precluding deoxycholate, which is much larger than zeatin, as a possible ligand. Among the residues interacting with the ligands, only Glu-69 (Asp-69 in Betv1) shows a conservation of chemical character. On the other hand, the ligand binding residues are nearly strictly conserved among the known CSBP sequences (Figure 9C).

An attempt at computational docking of a zeatin molecule into the cavity of Betv1 has been reported (Biesiadka et al., 2002). However, the location of the modeled ligand is completely different from that found experimentally in the structure described here. The docking algorithm placed the zeatin molecule at an additional entrance to the Betv1 cavity located between the Gly-rich loop L4 and the two short helices α1 and α2. In Vr CSBP, this site is plugged with a cluster of hydrophobic residues (Phe-26, Leu-54, Ile-71, and Ile-81), making it inaccessible to solvent or ligand molecules.

Biological Implications

A discussion of CSBP function cannot be separated from the mechanism of cytokinin action. Although in the past few years significant progress in cytokinin receptor identification has been made, there is still a lot to be learned. Molecular genetic screens in *Arabidopsis thaliana* revealed the presence of a membrane protein, CRE1, which acts as a cytokinin receptor (Inoue et al., 2001). The discovery of a membrane cytokinin receptor indicates that a receptor function of CSBPs, which are cytosolic, is unlikely.

The structural classification of CSBPs in one family with PR-10 proteins established in this study can form the basis for an educated guess about the elusive biological role of the latter class of pathogenesis-related proteins. The earlier suggestions that PR-10 proteins could function in the storage and/or transport of small-molecule ligands is strongly supported by their structural similarity to Vr CSBP. However, although the CSBPs have a clearly defined class of ligands, the natural small-molecule partners of the PR-10 proteins are still unknown. Comparison of the amino acid sequences among members of the CSBP group reveals that the residues forming hydrogen bonds with the invariant inner ligand are strictly conserved, except Leu-22, which binds zeatin via its main-chain carbonyl oxygen (Figure 9C). Also, the hydrophobic residues engaged in van der Waals interactions with the ligands are highly conserved. This indicates that all members of the CSBP family may bind cytokinins using the same mechanism. By contrast, in the PR-10 class, this would not be possible, as the ligand binding residues are not conserved between CSBP and PR-10 and as structural data show high variability in the shape and volume of their internal cavities. Another significant difference between CSBP and PR-10 proteins lies in their expression levels. The physiological concentration of CSBPs is very low, as expected for hormone binding proteins, whereas the PR-10 proteins are expressed at a much higher level.

It is possible that the CSBPs have evolved from the PR-10 group to specifically bind only one group of ligands, cytokinins. Because they are cytosolic proteins, a protective or transport function within the plant cell could be proposed. The low level of sequence conservation between the CSBP and PR-10 groups suggests early divergence or a fast mutation rate. In addition to mutations affecting the volume and chemical character of the ligand binding cavity, there are numerous other changes. Nevertheless, the evolutionary pressure has left the general protein fold intact, suggesting its importance and confirming a ligand binding role for PR-10 proteins.

Conclusions

In this atomic resolution structural study of cytokinin-specific binding protein from *V. radiata*, we have (1) established the structural basis for the classification of CSBPs in the PR-10 folding class. The high resolution of the electron density maps of

Table 4. Summary of Data Collection and Refinement Statistics

Data Collection	
Resolution limits (Å)	30.0 to 1.20 (1.22 to 1.20)[a]
Radiation source	BW7B beamline, EMBL/DESY
Temperature (K)	100
No. of measured reflections	1,277,993
No. of unique reflections	189,769
Redundancy	6.7 (4.5)
R_{int}[b]	0.070 (0.639)
Completeness (%)	95.7 (93.2)
$<I/\sigma(I)>$	19.7 (2.6)

Refinement	
Programs used	Refmac5/SHELXL
Resolution limits (Å)	15 to 1.2
Reflections	
Total	189,657
R_{free}	2,242
Rejection criteria	None
Atoms	
Protein	5,033
Ligand	146
Metal cations	2
Solvent	676
R/R_{free}[c]	
All reflections	0.157/0.190
$I>2\sigma(I)$	0.145/0.174
$<B>(Å^2)$	
Protein atoms	22.3
Zeatin atoms	
Inner	21.1
Outer	26.5
Intermolecular	27.6
Solvent atoms	32.6
rms deviation from ideality	
Bonds (Å)	0.020
Angles (°)	2.2
Ramachandran plot statistics (%)	
Most favored regions	90.2
Additionally allowed regions	9.8

[a] Values in parentheses correspond to the last resolution shell.
[b] $R_{int} = \Sigma_h\Sigma_j \mid I_{hj} - <I_h> \mid / \Sigma_h\Sigma_j I_{hj}$, where I_{hj} is the intensity of observation j of reflection h.
[c] $R = \Sigma_h \mid \mid F_o\mid - \mid F_c\mid \mid / \Sigma_h \mid F_o\mid$ for all reflections, where F_o and F_c are observed and calculated structure factors, respectively. R_{free} is calculated analogously for the test reflections, randomly selected, and excluded from the refinement.

this CSBP–zeatin complex has allowed (2) the precise determination of the protein–ligand interactions in the invariant cytokinin binding site. In addition, the crystal structure (3) has demonstrated that the binding pocket of CSBP can accept an additional zeatin molecule, which plugs the entrance to the binding pocket and seals the conserved ligand from contacts with bulk solvent. Finally, we have (4) reexamined the thermodynamics of cytokinin binding by CSBP, showing that the binding stoichiometry in solution corresponds to a 1:1 complex and that the K_d values are much higher than reported previously, covering the micromolar range.

METHODS

Spectroscopic and Calorimetric Measurements

Fluorimetric Titrations

All fluorimetric titrations were done at least in duplicate at 20°C using an FP-750 spectrofluorimeter (Jasco) equipped with a Peltier temperature-control unit under the following conditions: $\lambda_{exc} = 360$ nm, $\lambda_{em} = 480$ nm, using excitation and emission slit width of 5 nm. The fluorescence signal was corrected for the dilution factor. The concentrations of CSBP and ANS were determined spectrophotometrically using the molar extinction coefficients of 14,650 $M^{-1}\cdot cm^{-1}$ at 280 nm (calculated) (Pace et al., 1995) and 4990 $M^{-1}\cdot cm^{-1}$ at 350 nm (Mogensen et al., 2002), respectively.

ANS Binding to CSBP

Binding of ANS to *Vigna radiata* (Vr) CSBP was monitored by following the increase in fluorescence upon titration of a concentrated protein into a 1-cm × 1-cm stirred cuvette containing 1.2 mL of 10 mM MOPS buffer, pH 7.0, and 2.5 or 5.0 μM ANS. After addition of the ligand, each data point was collected after stabilization of the fluorescence signal (typically, 5 to 10 min). The data showed the hyperbolic shape and were fitted to the following equation by nonlinear least-squares analysis using the program Grafit 3.01 (Erithacus Software):

$$F_{obs} = \frac{F_{max}[protein]}{K_d + [protein]}, \tag{1}$$

where F_{obs} is the fluorescence signal, [protein] is the concentration of CSBP, K_d is the dissociation constant, and F_{max} is the fluorescence value at saturation.

ANS Displacement Assay

A preincubated mixture of 5.84 μM Vr CSBP and 8.5 μM ANS in 50 mM Tris, pH 7.0, at 20°C was used in cytokinin titration experiments. A stock solution of ANS was prepared in 10% DMSO. Because of very low solubility, stock solutions of the ligands were prepared in 100% dimethylformamide. The final concentration of dimethylformamide never exceeded 2.8% (v/v) in the protein samples. The mixture of CSBP and ANS was titrated with increasing ligand concentrations. After addition of the ligand, each data point was collected after stabilization of the fluorescence signal (typically, 5 to 10 min). The data were fitted to a sigmoidal dose–response equation to determine the EC_{50} value:

$$F_{obs} = F_{min} + \frac{F_{max} - F_{min}}{1 + 10^{(x-\log EC_{50})n}}, \tag{2}$$

where F_{obs} is the fluorescence signal, F_{max} is the maximal fluorescence in the absence of competing ligand, F_{min} is the residual ANS fluorescence when the CSBP is fully saturated with the ligand, EC_{50} is the ligand concentration for halfway dissociation of ANS from CSBP, and n (Hill slope) characterizes the stoichiometry and degree of interaction between the sites. The dissociation constants (K_d) of the CSBP–ligand complexes were derived from the approximate relationship between K_d and EC_{50} given by Cheng and Prusoff (1973):

$$K_d = \frac{EC_{50}}{1 + \frac{[ANS]}{K_d^{ans}}}, \tag{3}$$

where [ANS] is the ANS concentration in the displacement assay and K_d^{ans} is the CSBP–ANS dissociation constant determined in a separate experiment.

Calorimetric Titrations

Before the experiment, the protein solution was dialyzed extensively at 4°C against 20 mM phosphate buffer, pH 6.5. The titrations were performed using a Nano ITC 5300 instrument (Calorimetry Sciences). The titrated zeatin was dissolved to a concentration of 2.93 mM in dialysis buffer and injected in 8-μL aliquots. All experiments were done at 20°C. The ITC data were analyzed with Origin software to obtain the following thermodynamic parameters: stoichiometry (n), dissociation constant (K_d), and changes in the enthalpy and entropy of association (ΔH and ΔS, respectively). The heats of mixing were subtracted. The concentration of Vr CSBP was estimated using the molar extinction coefficient at 280 nm. The concentration of zeatin was estimated spectrophotometrically using the molar extinction coefficient $\varepsilon_{272} = 16{,}450$ M^{-1}·cm^{-1} (Letham et al., 1967).

Crystallographic Procedures

Before crystallization, zeatin was dissolved in 0.2 M HCl, and this zeatin solution (2.5 mM) was preincubated with protein solution at threefold molar excess of the ligand. Crystallization experiments were performed at room temperature using the hanging-drop vapor-diffusion method. The protein–ligand complex crystallized from high-salt precipitants containing 1.4 M sodium citrate and HEPES buffer, pH 7.5. The x-ray diffraction data were collected at the EMBL BW7B beamline at the DORIS ring of the DESY synchrotron. The protein crystallized in the $P6_4$ space group with unit cell parameters $a = 113.6$ and $c = 86.8$ Å. Details about crystallization, data collection, and preliminary data processing have been described (Bujacz et al., 2003). The statistics of data processing to 1.2 Å resolution are presented in Table 4.

The structure was solved by multiwavelength anomalous diffraction using the anomalous signal of tantalum introduced into the crystal in the form of a bromide salt of hexatantalum dodecabromide. The crystals were derivatized by soaking in 2.5 mM $(Ta_6Br_{12})Br_2$ solution for 36 h. The derivative crystals diffracted x-rays to 1.8 Å. In the final heavy-atom structure, five $(Ta_6Br_{12})^{2+}$ clusters were found. Initially, 22 tantalum sites were located by SOLVE (Terwilliger and Berendzen, 1999). The remaining eight sites were found in anomalous difference maps. The phases were further improved by density modification in DM (Cowtan, 1994). The model, built in ARP/wARP (Morris et al., 2002), contained almost all of the atoms present in the final structure, except for a *cis*-Pro peptide, the N-terminal Met, and a few C-terminal residues. Detailed description of the solution and refinement of the derivative crystal structure will be presented elsewhere.

The protein structure was refined using the native 15 to 1.2 Å data, first in Refmac5 (Murshudov et al., 1997) and then in SHELXL (Sheldrick and Schneider, 1997). The refinement was performed against all unique reflections, except 2242 reflections randomly selected for R$_{free}$ testing. Initially, several steps of isotropic refinement were conducted, combined with building of the ligand molecules. Stereochemical restraints for the zeatin molecule were imposed as for protein residues. A dictionary of ideal bond lengths and angles for zeatin was prepared in Refmac5 (Murshudov et al., 1997). The values for the purine ring were taken from neutral adenine description (as provided by a standard Refmac5 library). Water molecules were added if the corresponding F$_o$-F$_c$ peaks were higher than 4σ, and they were retained if their B-factors refined to <50 Å^2. Introduction of full anisotropic refinement decreased R and R$_{free}$ by 0.047 and 0.026, respectively. The occupancies of residues with dual conformation were adjusted manually based on electron density maps and temperature factors. In the last stages of refinement, hydrogen atoms at generated positions were included in the F$_c$ calculation. However, generation of hydroxyl H atoms of Ser, Thr, Tyr, and residues in double conformation was not activated. Also, no H atoms were attached to the zeatin molecules because of uncertainties concerning the protonation/tautomeric states. Throughout the refinement, manual model adjust-

ments, performed in XtalView (McRee, 1999), were based on 2F$_o$-F$_c$ and F$_o$-F$_c$ maps. The refinement results are summarized in Table 4.

Molecular and electron-density illustrations were prepared using the programs DINO (Philippsen, 2003) and PyMOL (DeLano, 2002).

Accession Numbers

Sequence data from this article can be found in the GenBank/EMBL data libraries under accession numbers AAC12790 (Ll PR-10.1A), AAC12791 (Ll PR-10.1B), CAB02159 (Betv1), BAA74451 (Vr CSBP), AAG00586 (Ll CSBP1), and AW234731 (Gm CSBP; the amino acid sequence was predicted from a cDNA clone). The structures discussed in this article are deposited in the Protein Data Bank under accession codes 1ICX (Ll PR-10.1A), 1IFV (Ll PR-10.1B), 1XDF (Ll PR-10.2A), 1BV1 (Betv1), and 1FM4 (Betv1 complex with deoxycholate). The structure described here, together with structure factors, has been deposited with the Protein Data Bank under accession code 2FLH.

REFERENCES

Biesiadka, J., Bujacz, G., Sikorski, M.M., and Jaskolski, M. (2002). Crystal structures of two homologous pathogenesis-related proteins from yellow lupine. J. Mol. Biol. **319,** 1223–1234.

Brese, N., and O'Keeffe, M. (1991). Bond-valence parameters for solids. Acta Crystallogr. B **47,** 192–197.

Bujacz, G., Pasternak, O., Fujimoto, Y., Hashimoto, Y., Sikorski, M., and Jaskolski, M. (2003). Crystallization and preliminary crystallographic studies of cytokinin-specific binding protein from mung bean. Acta Crystallogr. D **59,** 522–525.

Cheng, Y., and Prusoff, W.H. (1973). Relationship between the inhibition constant (K1) and the concentration of inhibitor which causes 50 per cent inhibition (I50) of an enzymatic reaction. Biochem. Pharmacol. **22,** 3099–3108.

Cohen, G.R. (1997). ALIGN: A program to superimpose protein coordinates, accounting for insertions and deletions. J. Appl. Crystallogr. **30,** 1160–1161.

Cowtan, K. (1994). Joint CCP4 and ESF-EACBM Newsletter on Protein Crystallography, Vol. 31. (Warrington, UK: Daresbury Laboratory).

DeLano, W.L. (2002). The PyMOL Molecular Graphics System (v0.99). Available at http://www.pymol.org.

Fujimoto, Y., Nagata, R., Fukasawa, H., Yano, K., Azuma, M., Iida, A., Sugimoto, S., and Shudo, K. (1998). Purification and cDNA cloning of cytokinin-specific binding protein from mung bean (*Vigna radiata*). Eur. J. Biochem. **258,** 794–802.

Gajhede, M., Osmark, P., Poulsen, F.M., Ipsen, H., Larsen, J.N., van Neerven, R.J.J., Schou, C., Lowenstein, H., and Spangford, M.D. (1996). X-ray and NMR structure of Bet v 1, the origin of birch pollen allergy. Nat. Struct. Biol. **3,** 1040–1045.

Inoue, T., Kiguchi, M., Hashimoto, Y., Seki, M., Kobayashi, M., Kato, T., Tabata, S., Shinozaki, K., and Kakimoto, T. (2001). Identification of CRE1 as a cytokinin receptor from *Arabidopsis.* Nature **409,** 1060–1063.

Iwamura, K., Fujita, T., Koyama, S., Koshimizmu, K., and Kumazawa, Z. (1980). Quantitative structure-activity relationship of cytokinin-active adenine and urea derivatives. Phytochemistry **19,** 1309–1319.

Kabsch, W. (1976). Rapid comparisons of protein structures. Acta Crystallogr. A **32,** 922–923.

Kobayashi, K., Fukuda, M., Igarashi, D., and Sunaoshi, M. (2000). Cytokinin-binding proteins from tobacco callus share homology with osmotin-like protein and an endochitinase. Plant Cell Physiol. **41,** 148–157.

Lee, B., and Richards, F.M. (1971). The interpretation of protein structures: Estimation of static accessibility. J. Mol. Biol. **55,** 379–400.

Letham, D.S. (1963). Zeatin, a factor inducing cell division isolated from *Zea mays.* Life Sci. **8,** 569–573.

Letham, D.S., Shannon, J.S., and McDonald, R.C. (1967). Regulators of cell division in plant tissues. III. The identity of zeatin. Tetrahedron **1,** 479–486.

Markovic-Housley, Z., Degano, M., Lamba, D., von Roepenack-Lahaye, E., Clemens, S., Susani, M., Ferreira, F., Scheiner, O., and Breiteneder, H. (2003). Crystal structure of a hypoallergenic isoform of the major birch pollen allergen Bet v 1 and its likely biological function as a plant steroid carrier. J. Mol. Biol. **325,** 123–133.

McRee, D.E. (1999). XtalView/Xfit—A versatile program for manipulating atomic coordinates and electron density. J. Struct. Biol. **125,** 156–165.

Mogensen, J.E., Wimmer, R., Larsen, J.N., Spangfort, M.D., and Otzen, D.E. (2002). The major birch allergen, Bet v 1, shows affinity for a broad spectrum of physiological ligands. J. Biol. Chem. **277,** 23684–23692.

Mok, D.W.S., and Mok, M.C. (1994). Cytokinins: Chemistry, Activity and Function. (Boca Raton, FL: CRC Press).

Morris, R.J., Perrakis, A., and Lamzin, V.S. (2002). ARP/wARP's model-building algorithms. I. The main chain. Acta Crystallogr. D **58,** 968–975.

Murshudov, G.N., Vagin, A.A., and Dodson, E.J. (1997). Refinement of macromolecular structures by the maximum-likelihood method. Acta Crystallogr. D **53,** 240–255.

Nayal, M., and Di Cera, E. (1996). Valence screening of water in protein crystals reveals potential Na^+ binding sites. J. Mol. Biol. **256,** 228–234.

Neudecker, P., Schweimer, K., Nerkamp, J., Scheurer, S., Vieths, S., Sticht, H., and Rosh, P. (2001). Allergic cross-reactivity made visible: Solution structure of the major cherry allergen Pru av 1. J. Biol. Chem. **276,** 22756–22763.

Pace, C.N., Vajdos, F., Fee, L., Grimsley, G., and Gray, T. (1995). How to measure and predict the molar absorption coefficient of a protein. Protein Sci. **4,** 2411–2423.

Pasternak, O., Biesiadka, J., Dolot, R., Handschuh, L., Bujacz, G., Sikorski, M.M., and Jaskolski, M. (2005). Structure of a yellow lupin pathogenesis-related PR-10 protein belonging to a novel subclass. Acta Crystallogr. D **61,** 99–107.

Philippsen, A. (2003). DINO: Visualizing Structural Biology (v0.9.0). Available at http://www.dino3d.org.

Romanov, G.A., Taran, V.Y., and Venis, M.A. (1990). Cytokinin-binding protein from maize shoots. J. Plant Physiol. **136,** 208–212.

Schirmer, T., Hoffimann-Sommergrube, K., Susani, M., Breiteneder, H., and Markovic-Housley, Z. (2005). Crystal structure of the major celery allergen Api g 1: Molecular analysis of cross-reactivity. J. Mol. Biol. **351,** 1101–1109.

Sheldrick, G.M., and Schneider, T.R. (1997). SHELXL: High-resolution refinement. Methods Enzymol. **227,** 319–343.

Terwilliger, T.C., and Berendzen, J. (1999). Automated MAD and MIR structure solution. Acta Crystallogr. D **55,** 849–861.

Thompson, J.D., Higgins, D.G., and Gibson, T.J. (1994). CLUSTAL W: Improving the sensitivity of progressive multiple sequence alignment through sequence weighting, position-specific gap penalties and weight matrix choice. Nucleic Acids Res. **22,** 4673–4680.

van Loon, L.C., and van Strien, E.A. (1999). The families of pathogenesis-related proteins, their activities and comparative analysis of PR-1 type proteins. Physiol. Mol. Plant Pathol. **55,** 85–97.

Wallace, A.C., Laskowski, R.A., and Thornton, J.M. (1995). LIGPLOT: A program to generate schematic diagrams of protein–ligand interactions. Protein Eng. **8,** 127–134.